MiR-129-3p regulates ferroptosis in the liver of Selenium-deficient broilers by targeting SLC7A11

Kaixin Zhang,* Xuedie Gu,* Yu Xia,* Xiaochun Zhao,[†] Ahmed Khoso Pervez,[‡] and Shu Li*,[1]

*College of Veterinary Medicine, Northeast Agricultural University, Harbin 150030, P. R. China; [†]Animal Disease Control and Prevention of Heilongjiang Province, Harbin 150069, China; and [‡]Shaheed Benazir Bhutto, University of Veterinary and Animal Sciences, Sakrand, Pakistan

ABSTRACT Selenium (**Se**) has been proven to be an essential trace element for organism. Se deficiency in poultry can cause widespread damage, such as exudative diathesis. The liver is not only the main organ of metabolism, but also one of the organs with high Se content in organism. Recent studies have shown that solute carrier family 7 member 11 (**SLC7A11**) plays a key role in the negative regulation of ferroptosis. In order to explore the mechanism of Se deficiency induces liver ferroptosis in broilers, and the role of micro-RNAs (**miRNAs**) in this process, we divided broilers into 2 groups: control group (0.2 mg/kg Se) and Se deficiency group (0.03 mg/kg Se). Hematoxylin-Eosin staining detected liver tissue damage in broilers. Predicted and verified the targeting relationship between miR-129-3p and SLC7A11 through miRDB and dual luciferase report experiments. The genes related to ferroptosis were detected by qRT-PCR and Western Blot. The results showed that the expression level of miR-129-3p mRNA in Se-deficient liver was significantly increased. To understand whether the miR-129-3p/SLC7A11 axis could involve in the process of ferroptosis, our further research showed that overexpression of miR-129-3p could reduce the expression of SLC7A11 and its downstream GCL, GSS, and GPX4, thereby inducing ferroptosis. These data indicates that miR-129-3p affected ferroptosis under Se deficiency conditions through the SLC7A11 pathway. Our research provides a new perspective for the mechanism of Se deficiency on the liver damage.

Key words: selenium deficiency, ferroptosis, miR-129-3p, SLC7A11, broiler liver

INTRODUCTION

Selenium (**Se**) is an essential trace element in the life of vertebrates (Xia et al., 2022). Se plays a vital role in the function of pathophysiology of various diseases, including diabetes (Kong and Song, 2021), cancer (Chu et al., 2004), cardiovascular disease (Kuria et al., 2020), and muscle metabolism (Chariot and Bignani, 2003). Se deficiency causes various damages to animal tissues, such as muscles (Rederstorff et al., 2006), nerves (Caito et al., 2011), immune organs (Zheng et al., 2018) and liver (Cai et al., 2022). Studies have shown that liver is not only the main organ of metabolism, but also one of the organs with high Se content in the organism (Liu et al., 2020). Dietary Se deficiency can cause liver damage, such as apoptosis (Liu et al., 2018).

Feeding mice with a low-Se diet, the Se content and glutathione activity in the liver were significantly reduced (Chiu-Ugalde et al., 2010). The lack of Se in the diet leads to the reduction of glutathione peroxidase 4 (**GPX4**). Previous research has shown GPX4 is critical for hepatocyte survival and proper liver function (Carlson et al., 2016). Dixon et al. found that ferroptosis is a unique form of cell death triggered by the oncogenic RAS-selective lethal small molecule Erastin. Ferroptosis is dependent on intracellular iron, but not on other metals, and is morphologically distinct from other cell death modes such as apoptosis (Dixon et al., 2012). Ferroptosis is regulated by a network revolving around GPX4 that could reduce lipid peroxides at the expense of GSH, and thus inhibit GPX4 are another major factor of small molecules that can induce ferroptosis. The activity of GPX4 is down-regulated, and a diet with insufficient Se can increase the sensitivity of ferroptosis and other death pathways (Cardoso et al., 2017). GPX4 converted lipid hydroperoxides to lipid alcohols, and this process prevents the iron dependent formation of toxic lipid reactive oxygen species (**ROS**). Inhibition of GPX4 function led to lipid peroxidation and could result in the

induction of ferroptosis (Forcina and Dixon, 2019). Depletion or inhibition of GPX4 using specific siRNA or the chemical inhibitor RSL3, respectively, resulted in the accumulation of lipid peroxide, leading to cell death by ferroptosis in H9C2 cardiomyoblasts (Park et al., 2019). GPX4 could regulate ferroptosis by inhibiting phospholipid peroxidation in Erastin and RSL3-induced ferroptosis (Imai et al., 2017). Therefore, it can be concluded that GPX4 is closely related to ferroptosis. Exploring ferroptosis in liver of broilers caused by Se deficiency can further enrich the research content of ferroptosis.

MicroRNAs (**miRNAs**), small (approximately $18-24$ nucleotides) and endogenous noncoding RNA molecules, regulate gene expression by destabilizing messenger RNA (**mRNA**) and/or repressing translation (Miao et al., 2022). MiRNA plays a regulatory role in key biological processes, such as embryonic development, cell proliferation, apoptosis, autophagy, mitochondrial function and immune response (Xu et al., 2021; Chen et al., 2022). Se deficiency affects the biological function of miRNA (Zhang et al., 2019). Se deficiency induced apoptosis of chicken liver by increasing the expression of miR-193b-3p (Liu et al., 2018). Study reported the regulation of miR-129 family on liver disease. For example, miR-129-5 inhibited liver fibrosis in mice (Ye et al., 2020). miR-129-2 reduced the proliferation and migration of liver cancer cells and stimulated their apoptosis (Wang et al., 2017). MiR-129-3p reduced Hepatocellular carcinoma (**HCC**) invasion in vitro and in vivo transfer (Cui et al., 2016). In addition, miR-129-3p can regulate cell death by targeting target genes to participate in the process of a variety of diseases. MiR-129-3p negatively targeted CPEB1 to facilitate chondrocyte viability and hamper apoptosis (Chen et al., 2020). Recent research found miR-129-3p favors intracellular *mycobacterium tuberculosis* survival in RAW264.7 cells by inhibiting autophagy via Atg4b (Qu et al., 2019). However, the mechanism of miR-129-3p involved in the regulation of ferroptosis need to be further explored.

As a specific light chain presenter of cysteine (**Cys2**)/glutamic acid (**Glu**) reversed transport protein, solute carrier family 7 member 11 (**SLC7A11**) plays a key role in the negative regulation of ferroptosis (Mou et al., 2019). SLC7A11 is a functional subunit of system Xc-, which was an important oncogenic protein that defended against oxidative stress and ferroptosis (Koppula et al., 2021). The expression of SLC7A11 induced ROS generation and oxidative stress by consuming nicotinamide adenine dinucleotide phosphate (**NADPH**) in the cell during the process of reducing the input L-cystine to L-cysteine (Joly et al., 2020).The inhibitory effect of SLC7A11 indirectly inactivated GPX4 and increased toxic lipid ROS by reducing the introduction of cystine and limiting the synthesis of GCL and GSS (Hassannia et al., 2019). Some studies have found that when transferrin receptor 1 (**TFR1**) charges cellular iron uptake, divalent metal transport protein 1 (**DMT1**) increased, causing iron overload and triggering cardiac ferroptosis (Lan et al., 2020). In addition, the transcription factor nuclear factor erythrocyte-like 2 related factor 2 (**NRF2**) was a key regulator of cellular antioxidant response (Zhao et al., 2021a). The accumulation of NRF2 causes Fe^{2+} to oxidize lipids in a Fenton-like manner, which led to the production of large amounts of ROS and promoted ferroptosis (Fei et al., 2020). Previous study found NRF2 overexpression or Keap1 knockdown in glioma cells accelerate proliferation and oncogenic transformation. Activation of the NRF2-KEAP1 signaling upregulates xCT and amplifies glutamate secretion. And KEAP1 inhibition promotes resistance to ferroptosis (Fan et al., 2017).

The purpose of this experiment was to study whether miRNA could regulate ferroptosis in the liver due to Se deficiency.

MATERIALS AND METHODS

Preparation of Animals and Sample Collection

All procedures used in this study were approved by the Institutional Animal Care and Use Committee (SRM-11) of Northeast Agricultural University. Forty healthy 1-day-old broilers were randomly divided into 2 groups: control group and Se deficiency group. The broilers were maintained on either adequate Se content diet (control group, 0.2 mg/kg Se) or Se deficiency diet (Se deficiency group, 0.03 mg/kg Se). After feeding the broilers for 42 d, we euthanized 40 broilers and quickly separated the liver tissues, part of which was put into fixative for fixation, and the remaining part was placed at $-80°C$ for use.

Histological Observation of Broiler Liver Tissue

To investigate the pathologic changes in liver tissue caused by Se deficiency, we fixed the tissue in 10% formalin phosphate solution, after trimming the tissue block, rinse with water for more than 12 h. Dehydration, transparent treatment, tissue block embedding treatment, the prepared tissue wax block is cut into 2 to 5 μm slices, spread out in warm water and fixed on a glass slide, and baked at 37°C for 12 h. Then, hematoxylin & eosin (**H&E**) staining for dewaxing and hydration dyeing, dehydrated with ethanol, transparent with xylene, and fixed with neutral gum for inspection.

Cell Culture and Treatment

The LMH (chicken hepatoma cells) line was gifted by Harbin Veterinary Research Institute, Chinese Academy of Agricultural Sciences. The cells were cultured and maintained in Dulbecco s modified Eagle's medium (**DMEM**; Gibco, Invitrogen, Carlsbad, CA) containing 10% fetal bovine serum (**FBS**; Gibco) in a humidified incubator containing 5% CO_2 at 39°C. To monitor the effects of Se on the LMH cells, the cells were treated for 24 h with 2 mg/mL sodium selenite (Li et al., 2008;

Table 1. The mimic and inhibitor sequences of gga-miR-129-3p.

Name	Sequences
Negative control	sense: 5'-UUCUCCGAACGU GUCACGUTT-3'
	antisense: 5'-ACGUGACACGUUC GGAGAATT-3'
MicroRNA inhibitor N.C	CAGUACUUUUGUGUAGUACAA
gga-miR-129-3p mimic	AAGCCCUUACCCCAAAAAGGAU
	CCUUUUUGGGGUAAGGGCUUUU
gga-miR-129-3p inhibitor	AUCCUUUUUGGGGUAAGGGCUU

Hu et al., 2020). The LMH cell in the 6-well plate grow to about 80%, discard the old medium and change to Opti medium. We used lip 2000 (Invitrogen, Carlsbad, CA) to compare mimics and inhibitors (GenePharma, Shanghai, China) (Table 1) to transfect LMH, cultured for 24 h, then cultured in normal medium for 12 h. For some experiments, the cells were treated with Erastin (an ferroptosis-inducing activator), Ferrostatin-1 (an Erastin-inducing ferroptosis inhibitor), for 24 h.

Dual Luciferase Reporter Assay

We constructed the pMIR-REPORT wild type (**WT**) and mutant type (**MT**) plasmids of the SLC7A11 3′UTR. SLC7A11 wild-type and mutant sequences are shown in Table 2. The WT and MT were as follows and cloned into the vector pMIR-REPORT. LMH were seeded into 24-well plates one day to transfection and transfected with WT or MT reporter vector, and expressed Renilla Photonase vectors pRL-TK and miR-129-3p mimic or negative controls. Luciferase activity was measured 24 h after transfection using the dual luciferase assay system (Promega, Madison, WI).

Cell Viability Assay

LMH was fed every day and subcultured once in culture flask to reach 90% to 100% confluence. Then the cells (3×10^3/well) were plated in 96-well plates and treated with treated with different concentrations of Erastin (0, 2.5, 5, 10, 20, and 40 μM) and Ferrostatin (0, 0.5, 1, 1.5, 2, and 2.5 μM) for 24 h. On the day of culture harvest, 10 mL CCK-8 was added to 90 mL of culture medium, and the cells were then incubated for 2 h at 39°C. After the absorbance was measured at 450 nm using an automatic microplate reader (BioTek Epoch, Winooski, VT). Cell viability was measured by using a CCK-8 kit (Dalian Meilun Biotechnology Co., Ltd.,

China). We chose 10 μM Erastin and 1 μM Ferrostatin-1 for the next experiments.

Malondialdehyde, Fe²⁺, and Glutathione Assay

According to the method of Kit instructions, the malondialdehyde9 (**MDA**), Fe^{2+} and glutathione (**GSH**) levels were measured by using corresponding commercial kits (NJJCBIO or Leagene, Beijing, China).

Detection of ROS

ROS production was measured by using a ROS Species Assay Kit (Beyotime, Shanghai, China). Cells were incubated with MDCFH-DA (10 μmol/L) in the dark for 30 min at 37°C. Cells were harvested and resuspended in Serum-free medium. Relative fluorescence intensity was evaluated by using fluorescence microscope.

Real-Time Quantitative PCR Analysis

The total RNA extraction kit is used to extract total RNA from tissues and cells. The OD260 / 280 of the extracted RNA was between 1.9 and 2.1, indicating purity of RNA can be conducted by following experiments. The cDNA First Strand Synthesis kit (Bioer Technology, Hangzhou, China) and miRcute miRNA First-strand cDNA Synthesis Kit (Tiangen Biotechnology, Beijing, China) are used to obtain complementary DNA (**cDNA**). The miRNA and mRNA first strand cDNA reverse transcription system were 20 μL for 42°C 60 min, 95°C 30 min; 10 μL for 37°C 20 min, 98°C 5 min, respectively. Then, qRT−PCR was carried out using SYBR Green (Roche, Basel, Switzerland) according to instructions. Data were analyzed using the $2^{-\Delta\Delta Ct}$ method by comparing with house-keeping gene, U6, and GAPDH, respectively. The primers used in this study were listed in Tables 3 and 4.

Western Blot Analysis

Proteins were extracted from cells and tissues via western IP (Beyotime, China) lysate. Protein samples, which were qualified with a BCA kit (Beyotime, Biotechnology), were separated via SDS-PAGE and then transferred onto PVDF membranes. After blocking in 5% milk for 2 h, the

Table 2. The gene sequences of SLC7A11 wild type and mutant type.

Name	Forward	Reverse
SLC7A11 WT	AGCTTCTAAGCATTGTGTAAGTAATAGT CAGGTGTACTGTGAAGAACGTATCCTAC CGTGAAGATCCTATTCGAGCT	CGAATAGGATCTTCACGGTAGGATACGT TCTTCACAGTACACCTGACTATTACTTA CACAATGCTTAGA
SLC7A11 MT	AGCTTCTAAGCATTGTGTAAGTAATAGT CAGGTGTTGACACTAGAACGTATCCTAC CGTGAAGATCCTATTCGAGCT	CGAATAGGATCTTCACGGT AGGATACGT TCTAGTGTCAACACCTGACTATTACTTA CACAATGCTTAGA

Table 3. mRNA primer sequences.

Name	Primer sequence (5′ → 3′)	Primer sequence (3′ → 5′)
SLC7A11	GCTGTCGTGAC GGTGCCTAATG	CTTCTCTTGTG GCTGCCTGCTG
GSS	GACTTCACGGCA CGGCTCTTC	CTGGCAGCGATG GTGTTGATCTC
GCL	GTGCCGAGGTGAT GGTGGATAAC	TGACTCCGACC ACACCGTACTG
GPX4	TCGGCCACCTCC ATCTACGAC	GTGCAGATCGACG AGCTGAGTG
TFR1	GTCAGAGGCAG CACCAAGAACC	GCAACGATAGCAT CAGGAGTCTCC
DMT1	ACATTGGAAGCA GCGGCAGTG	GGCAGCGACAA CAGCGTCTC
KEAP1	CAGCAGCGTGAGA GGTGAGTATG	CGGCGTACAGCA GTCGGTTC
NRF2	CAGGCCGTCTTGAA GCTCATCTC	CTTGCCTCTCCTGC GTATATCTCG
HO-1	ACGTCGTTGGCAA GAAGCATCC	TTGAACTTGGTGG CGTTGGAGAC
β-actin	CCGCTCTATGA AGGCTACGC	CTCTCGGCTGT GGTGGTGAA

Table 4. miRNA primer sequences.

Name	Primer sequence (5′ to 3′)
MiR-129-3p	CGAAGCCCTTACCCCAAAAAGGAT
U6	CACGCAAATTCGTGAAGCGTTCCA

PVDF membranes were incubated with primary antibody overnight. Subsequently, secondary antibody was used to incubate the membrane at 37°C for 1.5 h. The protein bands were visualized using chemiluminescence and bands intensities were calculated. The primary antibodies and source are presented in Table 5.

Statistical Analysis

All data in our study were presented as the mean ± SD. GraphPad Prism software (version 8.0, San Diego, CA) was used to analyze the data. The Tukey test in one-way ANOVA analysis was used to compare the differences between the control group and the selenium deficiency group. Differences were considered to be significant at $P < 0.05$ and highly significant at $P < 0.01$.

Table 5. The information of primary antibodies.

Name	Source	Identifier	Dilution ratio
SLC7A11	ABclonal	A13685	1:800
GCL	Bioss	bs-8402R	1:1,000
GSS	Affinity	DF6214	1:500
GPX4	Bioss	bs-3884R	1:500
TFR1	Wanleibio	WL03500	1:1,000
DMT1	Wanleibio	WL05401	1:1,000
KEAP1	Wanleibio	WL03285	1:2,000
NRF2	Wanleibio	WL02135	1:500
HO-1	Wanleibio	WL02400	1:1,500
GAPDH	Wanleibio	WL01114	1:800

RESULTS

Histological Observation of Broiler Liver Tissue

In order to study the effect of Se deficiency on the liver, we established a Se deficiency broiler model, we found that broilers in the Se deficiency group had obvious clinical symptoms of exudative diathesis, and tested Se contents and activities of GSH-PX in the serum and liver of broilers, we found that the Se concentration and the activity of GPx in the Se deficiency group were significantly lower than Control group (Table S1). We performed pathological observations on liver tissue as shown in Figure 1. Observation under the microscope showed that the liver lobules of the control group were clearly structured, the liver cords were neatly arranged, and the liver cells were arranged in a single layer in clusters or cords. The cell membrane had clear boundaries, abundant cytoplasm, fine granular shape, and clear nuclear structure. In the Se deficiency group, hepatic cords were arranged disorderly, hemorrhages, intercellular spaces became enlarged, liver cells were abnormal, inflammatory cell infiltration, and adipose cell degeneration occurred.

MiR-129-3p Directly Targets and Regulates SLC7A11

In order to understand how miR-129-3p triggered ferroptosis in the liver, we used real-time quantitative PCR to detect the expression of miR-129-3p in broiler liver tissue. The results of qRT-PCR showed that compared with the control group, the expression of miR-129-3p was significantly increased, and the increase was 2.6 times of the original ($P < 0.01$; Figure 2A). Then we got 327 target genes about miR-129-3p by the miRDB website prediction, and selected which target score was higher and was related to ferroptosis genes. The miRDB website predicted SLC7A11 as one of the target genes of miR-129-3p (Figure 2B). To verify the targeting relationship between miR-129-3p and SLC7A11, we constructed the WT or MT 3′UTR of SLC7A11 to the pMIR-REPORT plasmids (Figure 2C) and co-transfected them into LMH cells with miR-129-3p mimics or negative control or inhibitor negative control for optimal transfection concentration (Figure 2D). The miR-129-3p mimics observably decreased the luciferase activity of the WT 3′UTR of SLC7A11 ($P < 0.01$). However, when miR-129-3p co-transfected with MT 3′UTR of SLC7A11, the luciferase activity did not differ significantly comparing with negative control group (Figure 2E), which suggested that miR-129-3p directly targets to the 3′UTR of SLC7A11.

In addition, it is necessary to further study whether Se deficiency affects the expression of SLC7A11 in broiler liver tissue. The results showed that the mRNA level of SLC7A11 in the Se-deficiency group was lower than that control group by qRT-PCR ($P < 0.05$), and the protein expression level was significantly lower comparing with
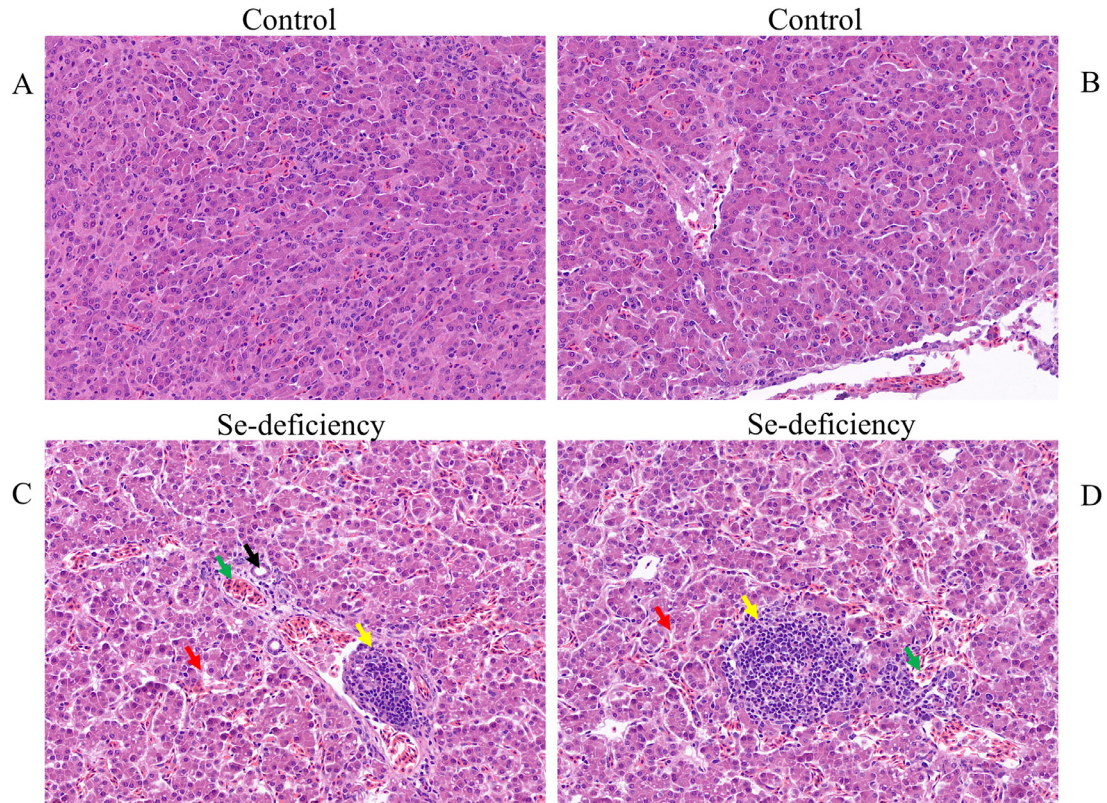
Figure 1. Histopathological changes in the liver tissue of broilers. Hematoxylin-eosin staining (HE) of broiler liver, hepatocytes of broiler liver tissue are disorderly arranged, hemorrhage (green arrow), intercellular space enlargement (red arrow), inflammatory cell infiltration (yellow arrow) and adipose cell degeneration (black arrow).

control group by Western blot ($P < 0.01$; Figures 2F and 2G). It confirmed that the expression of SLC7A11 was significantly reduced in the liver tissue of Se-deficient broilers.

LMH were transfected with miR-129-3p mimic and miR-129-3p inhibitor respectively, and the mRNA and protein expressions of SLC7A11 in LMH were affected. The results showed in Figures 2H and 2I, the mRNA expression of SLC7A11 in the mimic group was significantly lower than that in the control group, and the protein expression was also significantly lower ($P < 0.01$). On the contrary, the mRNA and protein expression of SLC7A11 in the inhibitor group were significantly higher than those in the control group ($P < 0.01$). In summary, these results indicated that SLC7A11 was a specific downstream target gene of miR-129-3p.

The Effect of miR-129-3p Overexpression on Erastin-Induced LMH Lipid Metabolism

First, LMH was treated with different concentrations of Erastin, and its activity was measured with CCK-8, according to the results, the dose of Erastin was used 10 μM and Ferrostatin-1 was used 1 μM finally. And we found that Erastin significantly reduced the vitality of LMH in a dose-dependent manner (Figure 3A). Ferrostatin-1 could reverse Erastin-induced cell death (Figure 3A). The changes in indicators related to ferroptosis in LMH were determined by commercial kits. Results showed that the level of MDA and Fe^{2+} in the

LMH of miR-129-3p with Erastin was increased and they significantly increased comparing with miR-129-3p group alone (Figures 3B and 3C). In addition, the levels of those were reversed in Ferrostatin-1 group. Except for that, the level of antioxidant GSH reduced more comparing with miR-129-3p group alone (Figure 3D), the expression of GSH slightly returned in Ferrostatin-1 group. ROS is one of the essential factors that lead to ferroptosis, therefore, the level of ROS in LMH was detected by fluorescence microscopy. As shown in Figure 3E, in the presence of miR-129-3p increased the production of ROS. The increase of ROS was more obvious in the Erastin + miR-129-3p group, and ROS levels almost returned to normal levels after adding Ferrostatin-1. The results indicated that the overexpression of miR-129-3p enhanced the lipid oxidation induced by Erastin in LMH.

Se Deficiency Activates the SLC7A11/GPX4 Pathway

In vivo, the mRNA expressions of SLC7A11, GCL, GSS, and GPX4 related to ferroptosis in broiler liver tissue were detected. qRT-PCR results showed that compared with the control group, GCL, GSS, and GPX4 were decreased by 25, 45, 55% respectively. GPX4 decreased most significantly ($P < 0.05$; Figure 4A). The protein expression trend of those genes was consistent with the mRNA expression. The expression of GPX4 was down-regulated most significantly, by 25% after quantification ($P < 0.05$; Figures 4B and 4C).
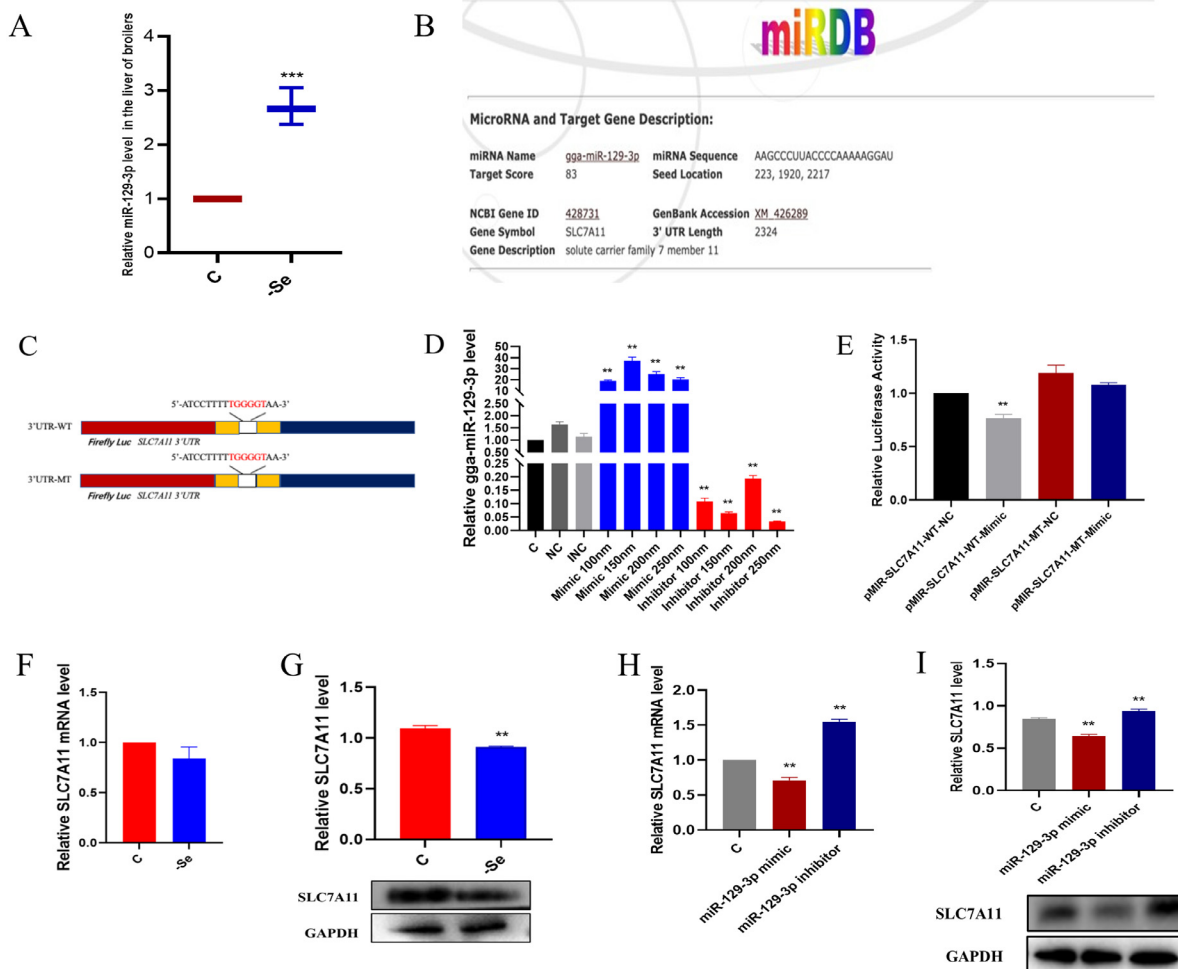
Figure 2. SLC7A11 is the target gene of miR-129-3p. (A) The miRDB website predicts that SLC7A11 may be the direct target gene of miR-129-3p. (B) qRT-PCR to detect the mRNA expression of miR-129-3p in the control group and the Se-deficient group. (C) Clone the WT and MT of the SLC7A11 3′UTR sequence into the pMIR-REPORT plasmid. (D) In LMH cells, different concentrations of mimics and inhibitors are used for transfection to determine the optimal transfection concentration. (E) Determination of dual luciferase reporter gene. Transfect broiler kidney primary cells with WT or MT SLC7A11 3′UTR and negative control (NC) miR-129-3p mimic. The relative luciferase expression of firefly is normalized to Renilla luciferase. (F) qRT-PCR to detect the mRNA expression of SLC7A11 in the control group and the Se deficiency group. (G) Western Blot detects the protein expression of SLC7A11 in the control group and the Se deficiency group. (H) qRT-PCR detection of the mRNA expression of SLC7A11 in miR-129-3p mimic and miR-29-3p inhibitor in the control group. (I) Western Blot detection control group qRT-PCR detection control group, miR-129-3p mimic and miR-29-3p inhibitor group SLC7A11 protein expression.. Data are expressed as mean ± SD (n = 6). $P < 0.05$, $P < 0.01$. Abbreviations: I, miR-129-3p inhibitor; M, miR-129-3p mimic

In LMH cells, the mRNA and protein content of SLC7A11, GCL, GSS, and GPX4 genes were detected respectively. The results showed that the expression of SLC7A11, GCL, GSS, and GPX4 genes in the miR-129-3p group were decreased ($P < 0.05$), and those in the Erastin + miR-129-3p group decreased more significantly than miR-129-3p group ($P < 0.05$), no matter what protein and mRNA level. However, the mRNA expressions of SLC7A11, GCL, GSS, and GPX4 slightly increased after the addition of Ferrostatin-1 (Figure 4D). At the same time, protein expression was detected by Western blotting (Figures 4E and 4F). The results were consistent with qRT-PCR. The above results indicated that miR-129-3p lead to negative regulation on SLC7A11/GPX4 pathway-related genes, and the addition of Ferrostatin-1 could partially reverse this effect. It also indicated that miR-129-3p could induce ferroptosis by targeting SLC7A11 to regulate the SLC7A11/GPX4 pathway.

Se Deficiency Activates the TFR1/DMT1 Pathway

TFR1/DMT1 is also another signal pathway to modulate Ferroptosis. The mRNA expressions of TFR1 and DMT1 in broiler liver tissue were detected. qRT-PCR results showed that TFR1 and DMT1 were increased 1.5 times and 1.4 times respectively in Se deficiency group ($P < 0.05$), comparing with control group (Figure 5A). The protein expression level of TFR1 and DMT1 were consistent with the mRNA expression ($P < 0.05$; Figures 5B and 5C).

In LMH cells, the mRNA and protein content of TFR1 and DMT1 genes were detected respectively. The results showed that the mRNA and protein expression levels of TFR1 and DMT1 genes in miR-129-3p group were increased ($P < 0.05$), and those in Erastin + miR-129-3p group increased more significantly than miR-129-3p group ($P < 0.05$). However, the mRNA
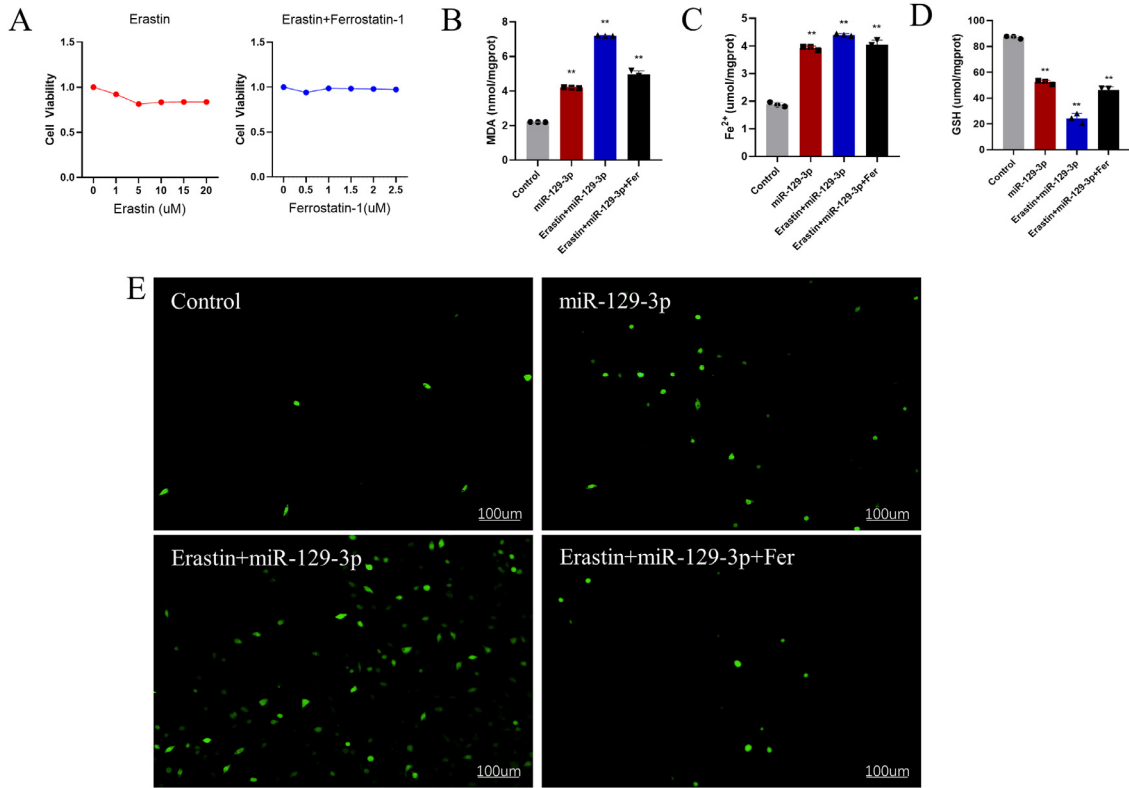
Figure 3. The effect of miR-129-3p overexpression on Erastin-induced LMH lipid metabolism. (A) CCK-8 measures the viability of LMH cells in Erastin and Erastin + Ferrostatin-1 groups. (B) qRT-PCR was used to determine the mRNA expression level of MDA in the control group, miR-129-3p group, Erastin + miR-129-3p group, and Erastin + miR-129-3p + Ferrostatin-1 group. (C) The expression of Fe^{2+} in the control group, miR-129-3p group, Erastin + miR-129-3p group, Erastin + miR-129-3p + Ferrostatin-1 group was determined by qRT-PCR. (D) The mRNA expression level of GSH in the control group, miR-129-3p group, Erastin + miR-129-3p group, Erastin + miR-129-3p + Ferrostatin-1 group was determined by qRT-PCR. (E) The expression level of ROS in the control group, miR-129-3p group, Erastin + miR-129-3p group, Erastin + miR-129-3p + Ferrostatin-1 group.
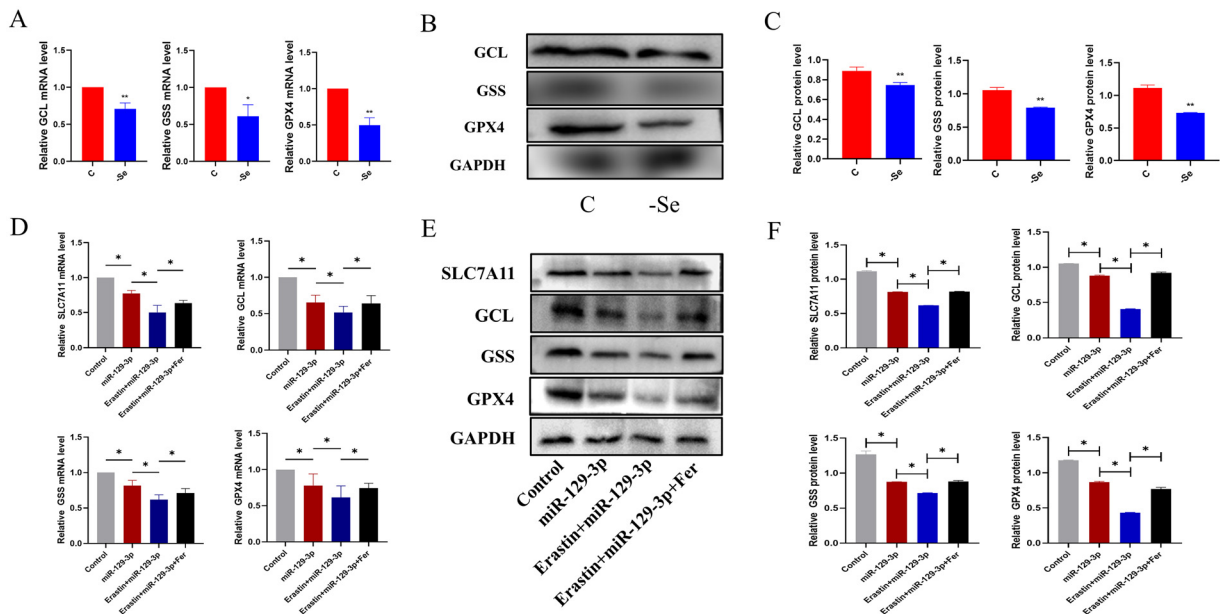
Figure 4. The mRNA and protein levels of SLC7A11/GPX4 pathway related genes in broiler liver. (A) The mRNA levels of GCL, GSS and GPX4 in the liver tissue of broilers in the control group and the Se deficiency group. (B−C) The protein levels of GCL, GSS and GPX4 in the liver tissue of broilers in the control group and the Se deficiency group. (D) The mRNA levels of miR-129-3p group, Erastin + miR-129-3p group, Erastin + miR-129-3p + Ferrostatin-1 group and control group GCL, GSS and GPX4 in liver tissues of broilers. (E−F) The protein levels of miR-129-3p group, Erastin + miR-129-3p group, Erastin + miR-129-3p + Ferrostatin-1 group and control group GCL, GSS and GPX4 in liver tissues of broiler broilers. Each value represents the mean ± SD (n = 6). *There is a significant difference between the Se deficiency group and the control group, miR-129-3p group, Erastin + miR-129-3p group, Erastin + miR-129-3p + Ferrostatin-1 group and the control group have significant differences ($P < 0.01$).
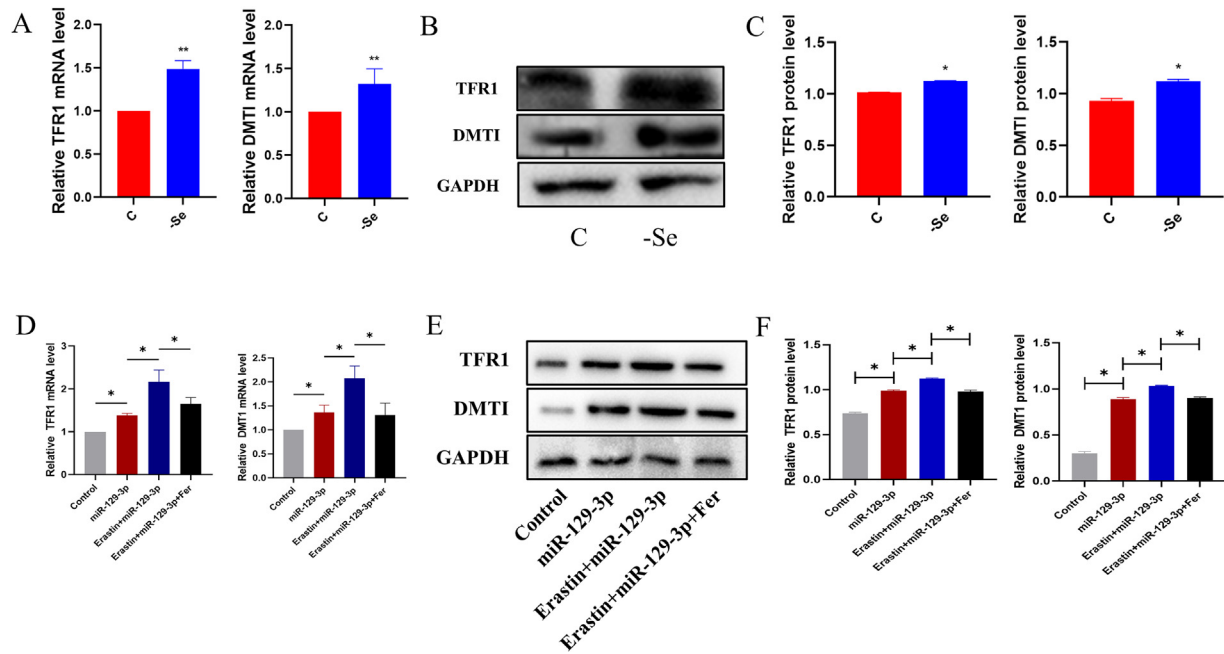
Figure 5. The mRNA and protein levels of genes related to the TFR1/DMT1 pathway in broiler liver. (A) The mRNA levels of TFR1 and DMT1 in the liver tissue of broiler broilers in the control group and the Se deficiency group. (B–C) The protein levels of TFR1 and DMT1 in the liver tissue of broiler in the control group and the Se deficiency group. (D) The mRNA levels of miR-129-3p group, Erastin + miR-129-3p group, Erastin + miR-129-3p + Ferrostatin-1 group and control group TFR1 and DMT1 in liver tissues of broilers. (E–F) Protein levels of miR-129-3p group, Erastin + miR-129-3p group, Erastin + miR-129-3p + Ferrostatin-1 group and control group TFR1 and DMT1 in liver tissues of broilers. Each value represents the mean ± SD (n = 6). *There is a significant difference between the Se deficiency group and the control group, miR-129-3p group, Erastin + miR-129-3p group, Erastin + miR-129-3p + Ferrostatin-1 group and the control group have significant differences ($P < 0.01$).

expressions of TFR1 and DMT1 decreased after the exposed to Ferrostatin-1, and restored to normal level (Figure 5D). At the same time, protein expression was detected by Western blotting (Figures 5E and 5F). The result was consistent with qRT-PCR. The above results indicated that the expression of miR-129-3p increases can lead to ferroptosis in liver, and then activates TFR1/DMT1 signal pathway to promote the expression of ferroptosis related genes.

Se Deficiency Activates the KEAP1/HO-1 Pathway

The mRNA expressions of KEAP1/HO-1 related to ferroptosis in broiler liver tissue were detected. qRT-PCR results showed that compared with the control group, KEAP1 increased 1.49 times, while NRF2 and HO-1 were decreased by 80% and 50% respectively ($P < 0.05$; Figure 6A). The results of protein expression level were consistent with the mRNA expression ($P < 0.05$; Figure 6B and 6C).

In LMH cells, the mRNA and protein content of KEAP1, NRF2 and HO-1 genes were detected respectively. The results showed that KEAP1 in the miR-129-3p group were increased ($P < 0.05$), and it in the Erastin + miR-129-3p group increased more significantly than miR-129-3p group ($P < 0.05$). While mRNA expressions of KEAP1 decreased after the addition of Ferrostatin-1, and tended to normal levels. However, NRF2 and HO-1 in the miR-129-3p group were

decreased ($P < 0.05$), and those in the Erastin + miR-129-3p group decreased more significantly than miR-129-3p group ($P < 0.05$). While the mRNA expressions of NRF2 and HO-1 increased after the addition of Ferrostatin-1 (Figure 6D). At the same time, protein expression was detected by Western blotting (Figures 6E and 6F). The results are consistent with qRT-PCR. The above results indicated that miR-129-3p could promote the reduction effect of Erastin on KEAP1/HO-1 pathway-related genes, and the addition of Ferrostatin-1 could partially reverse this effect.

DISCUSSION

Se exerted many biological protective functions to maintain the body's normal homeostasis (Payne and Southern, 2005). Se deficiency in the diet can cause liver damage, and the liver is the main target organ for Se deficiency. Therefore, this has important reference significance for liver diseases related to Se deficiency. Under the condition of Se deficiency, we found that miR-129-3p plays a role in the metabolic pathway of ferroptosis, and it is for the first time to confirm in vivo and in vitro that miR-129-3p regulates intracellular lipid metabolism, SLC7A11 and its downstream molecules to enhance the ferroptosis in liver.

Se deficiency leads to a variety of liver injury. Studies have shown that Se deficiency can cause liver damage in rats, including pathological changes and fibrosis of hepatic portal vein (Han et al., 2017). In this study, the
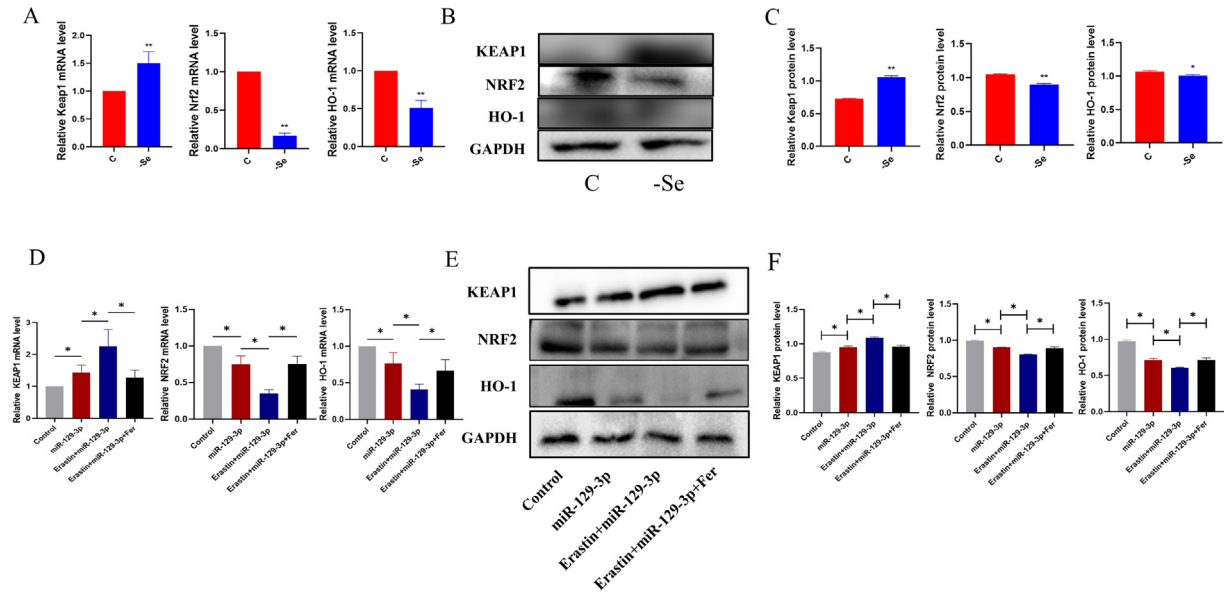
Figure 6. The mRNA and protein levels of KEAP1/HO-1 pathway related genes in broiler liver. (A) The mRNA levels of KEAP1, NRF2 and HO-1 in the control group and the Se deficiency group in broiler liver tissues. (B−C) The protein levels of KEAP1, NRF2 and HO-1 in the liver tissue of broiler in the control group and the Se deficiency group. (D) The mRNA levels of miR-129-3p group, Erastin + miR-129-3p group, Erastin + miR-129-3p + Ferrostatin-1 group and control group KEAP1, NRF2 and HO-1 in liver tissues of broilers. (E−F) Protein levels of miR-129-3p group, Erastin + miR-129-3p group, Erastin + miR-129-3p + Ferrostatin-1 group and control group KEAP1, NRF2 and HO-1 in liver tissues of broiler broilers. Each value represents the mean ± SD (n = 6). *There is a significant difference between the Se deficiency group and the control group, miR-129-3p group, Erastin + miR-129-3p group, Erastin + miR-129-3p + Ferrostatin-1 group and the control group have significant differences ($P < 0.01$).

results of microstructure of liver in Se-deficient broilers, comparing with control group, it showed many typical characteristics with disordered arrangement of hepatocytes, hemorrhage, enlarged intercellular space, inflammatory cell infiltration and adipocyte degeneration. Ferroptosis is the form of regulated cell death (**RCD**) characterized by iron-dependent lipid peroxidation (Dixon et al., 2012). The import of oxidized cysteine (cystine) via system Xc- is a critical dependency of pancreatic ductal adenocarcinoma (**PDAC**). As a system Xc- subunit, the deletion of SLC7A11 induced tumor-selective ferroptosis and inhibited PDAC (Badgley et al., 2020). GPX4, the downstream factor of SLC7A11, is the only enzyme that could use GSH as an electron donor to reduce the toxic lipid hydroperoxide in the biofilm to the corresponding alcohol (Kim et al., 2020). Inactivation of GPX4 or depletion of GSH in cells can cause ferroptosis (Guan et al., 2021). Previous studies showed that Se deficiency induced ferroptosis by reducing the expression of GPX4. Zhao et al. found that Se deficiency decreased the expression of GPX4 in chicken heart, and then down-regulated the expression of SLC7A11, resulting in ferroptosis in chicken cardiomyocytes (Zhao et al., 2021b). In this study, we found the expression level of SLC7A11/GPX4 axis in Se deficiency model was down-regulated as in previous studies.

In previous studies, it indicated that Se deficiency can affect the expression level of multiple miRNAs in the liver of broilers. Among the expression of 8 kinds of miRNA in the liver of broilers, miR-193b-3p increased most significantly, which is discovered by researchers. In addition, miR-193b-3p could regulate hepatocyte apoptosis by targeting MAML1 in Se-deficient broilers

(Liu et al., 2018). In this study, we found that Se deficiency led to a significant increase in mRNA expression of miR-129-3p. Although there are no studies to describe involvement of miR-129-3p in ferroptosis, it has been widely studied on the regulation of cell death by miR-129-3p. Previous study found that overexpression of Smad3 reversed the inflammation and apoptosis by inhibiting the expression of miR-129-3p in PA-stimulated cardiomyocytes (Zou and Kong, 2019). Circ-SETDB1 silencing repressed serous ovarian cancer malignant progression through miR-129-3p/MAP3K3 pathway (Li and Zhang, 2021). In this study, due to obviously increase the expression of miR-129-3p in the liver of broilers, which it affects expression of related downstream genes to cause liver injury, it needs to be further study to verify the pathological role related to ferroptosis.

After determining the most differentially expressed miR-129-3p in broiler liver, the target gene SLC7A11 of miR-129-3p was further screened and identified through the target gene prediction website and double luciferase report. The level of SLC7A11 could be inhibited by different stimuli. For example, the p53 3KR mutant binds to the promoter of the SLC7A11 gene and inhibits the expression of SLC7A11, thereby inhibiting the uptake of cystine and promoting hypertrophy (Liu et al., 2019). BECN1 directly blocks the activity of system Xc- by combining with core component SLC7A11 to promote hypertrophy (Koppula et al., 2018). In this study, miR-129-3p was observed significantly decrease the luciferase activity of 3′UTR in WT of SLC7A11 by dual luciferase reporter experiments. However, regulatory relationship of that was lost by constructing the mutagenesis of

3′UTR in SLC7A11. In addition, it was found that the expression of SLC7A11 was significantly decreased in miR-129-3p mimic group, while the expression of SLC7A11 was significantly increased in miR-129-3p inhibitor group. It confirmed that there was a targeted relationship between miR-129-3p and SLC7A11, and miR-129-3p could negatively regulate SLC7A11. As a functional subunit of system Xc-, SLC7A11 was an important protein that can resist oxidative stress and ferroptosis. With the decrease in SLC7A11 expression, it led to the decrease in GCL, GSS, and GPX4 expression, finally, led to the increase of ROS to promote the occurrence of ferroptosis. In summary, our findings described the role of miR-129-3p in promoting ferroptosis in broilers liver.

Overexpression of miR-129-3p, co-transfecting with Erastin, which caused LMH more sensitive to ferroptosis by affecting expression level of SLC7A11. Erastin is an activator of ferroptosis. It consumed glutathione (a major cellular antioxidant), leading to the accumulation of ROS (Lee et al., 2020; He et al., 2022; Tang et al., 2022). We observed that by measuring the changes in these lipid oxidation-related molecules, miR-129-3p promoted the lipid oxidation of liver cancer cells. Interestingly, we further found that miR-129-3p strongly promotes cell death induced by Erastin. Our results showed that transfected miR-129-3p mimic into Erastin-treated LMH cells, the expression levels of GCL, GSS, and GPX4 were significantly decreased in the Erastin+miR-129-3p group, comparing with control and miR-129-3p group. This indicated that miR-129-3p could aggravate the ferroptosis induced by Erastin through SLC7A11/GPX4 signal pathway depended on accumulating ROS. Our research showed that miR-129-3p further enhanced the reduction of GSH and the accumulation of ROS and MDA in LMH induced by protein kinase. Our findings described the essential role of miR-129-3p in promoting ferroptosis in LMH.

Legal Fe(II) is essential for hypertrophy due to promote the production of lipid peroxides (Zhang et al., 2020). As a transmembrane receptor protein, TFR1 binds to the iron transporter transferrin and assists iron uptake through endocytosis. Divalent metal transporter 1 (**DMT1**) has been identified as a non-transferrin-bound serum iron (**NTBI**) pathway and was responsible for the absorption of ferrous iron. DMT1 was also located on the cell membrane surface and could transport extracellular ferrous ions (Chen et al., 2019). Our results indicated that Se deficiency led to the increase of expression of TFR1 and DMT1. In vitro, miR-129-3p further enhanced the expressions of TFR1 and DMT1 induced by Erastin. More and more studies have shown that HO-1 played a key role in ferroptosis (Kwon et al., 2015). HO-1 promoted iron promotion by releasing its enzymatic product iron, which was related to cellular stress caused by lipid ROS and glutathione depletion (Adedoyin et al., 2018). Specifically, the nuclear localization of HO-1 has been shown to be different

experimental conditions, and could be used to up-regulate cytoprotective genes against oxidative stress (He et al., 2022). The activation of HO-1 also depends on other transcription factors, including the KEAP1/NRF2 pathway (Wu et al., 2019). Our results showed that Se deficiency causes the expression levels of TFR1, DMT1, NRF2 and HO-1 were significantly increased and KEAP1 were significantly decreased in liver of broilers. And in LMH, the expression levels of TFR1, DMT1, NRF2 and HO-1 were significantly increased in miR-129-3p group and Erastin+miR-129-3p group. KEAP1 were significantly decreased in miR-129-3p group and Erastin +miR-129-3p group. These results indicated that Se deficiency can regulate the expression of ferroptosis pathway-related genes and cause ferroptosis by regulating the expression of miR-129-3p.

CONCLUSIONS

In summary, our results indicated that Se deficiency could significantly increase the expression of miR-129-3p, miR-129-3p regulated the GCL/GSS/GPX4 axis by targeting SLC7A11, resulting in an increase in ROS to induce ferroptosis. In addition, Se deficiency led to elevated expression levels of ferroptosis-related genes including TFR1, DMT1 and other genes. This study demonstrated that Se deficiency could cause ferroptosis by regulating the miR-129-3p/SLC7A11 axis, and provided a basis for the prevention and treatment of diseases related to Se deficiency.

ACKNOWLEDGMENTS

DISCLOSURES

All the authors declared that there were no conflicts of interest.

SUPPLEMENTARY MATERIALS

Supplementary material associated with this article can be found in the online version at doi:10.1016/j.psj.2022.102271.

REFERENCES

Adedoyin, O., R. Boddu, A. Traylor, J. Lever, S. Bolisetty, J. George, and A. Agarwal. 2018. Heme oxygenase-1 mitigates ferroptosis in renal proximal tubule cells. Am. J. Physiol. Renal Physiol. 314: F702–F714.

Badgley, M. A., D. M. Kremer, H. C. Maurer, K. E. DelGiorno, H. J. Lee, V. Purohit, I. R. Sagalovskiy, A. Ma, J. Kapilian, C. E. M. Firl, A. R. Decker, S. A. Sastra, C. F. Palermo, L. R. Andrade, P. Sajjakulnukit, L. Zhang, Z. P. Tolstyka, T. Hirschhorn, C. Lamb, T. Liu, W. Gu, E. S. Seeley, E. Stone, G. Georgiou, U. Manor, A. Iuga, G. M. Wahl, B. R. Stockwell, C. A. Lyssiotis, and K. P. Olive. 2020. Cysteine depletion induces pancreatic tumor ferroptosis in mice. Science (New York, N.Y.) 368:85–89.

Cai, J., J. Huang, J. Yang, X. Chen, H. Zhang, Y. Zhu, Q. Liu, and Z. Zhang. 2022. The protective effect of selenoprotein M on nonalcoholic fatty liver disease: the role of the AMPKα1-MFN2 pathway and Parkin mitophagy. Cell. Mol. Life Sci. 79:354.

Caito, S., D. Milatovic, K. Hill, M. Aschner, R. Burk, and W. Valentine. 2011. Progression of neurodegeneration and morphologic changes in the brains of juvenile mice with selenoprotein P deleted. Brain Res. 1398:1–12.

Cardoso, B., D. Hare, A. Bush, and B. Roberts. 2017. Glutathione peroxidase 4: a new player in neurodegeneration? Mol. Psychiatry 22:328–335.

Carlson, B. A., R. Tobe, E. Yefremova, P. A. Tsuji, V. J. Hoffmann, U. Schweizer, V. N. Gladyshev, D. L. Hatfield, and M. Conrad. 2016. Glutathione peroxidase 4 and vitamin E cooperatively prevent hepatocellular degeneration. Redox Biol. 9:22–31.

Chariot, P., and O. Bignani. 2003. Skeletal muscle disorders associated with selenium deficiency in humans. Muscle Nerve 27:662–668.

Chen, C., P. Liu, X. Duan, M. Cheng, and L. Xu. 2019. Deferoxamine-induced high expression of TfR1 and DMT1 enhanced iron uptake in triple-negative breast cancer cells by activating IL-6/PI3K/AKT pathway. OncoTargets Ther. 12:4359–4377.

Chen, D., Y. Yao, X. Shi, X. Li, W. Cui, and S. Xu. 2022. Cadmium exposure causes mitochondrial fission and fusion disorder in the pig hypothalamus via the PI3K/AKT pathway. Ecotoxicol. Environ. Saf. 242:113880.

Chen, R., B. Ye, H. Xie, Y. Huang, Z. Wu, H. Wu, X. Wang, H. Miao, and W. Liang. 2020. miR-129-3p alleviates chondrocyte apoptosis in knee joint fracture-induced osteoarthritis through CPEB1. J. Orthop. Surg. Res. 15:552.

Chiu-Ugalde, J., F. Theilig, T. Behrends, J. Drebes, C. Sieland, P. Subbarayal, J. Köhrle, A. Hammes, L. Schomburg, and U. Schweizer. 2010. Mutation of megalin leads to urinary loss of selenoprotein P and selenium deficiency in serum, liver, kidneys and brain. Biochem. J. 431:103–111.

Chu, F. F., R. S. Esworthy, and J. H. Doroshow. 2004. Role of Se-dependent glutathione peroxidases in gastrointestinal inflammation and cancer. Free Radic. Biol. Med. 36:1481–1495.

Cui, S., K. Zhang, C. Li, J. Chen, Y. Pan, B. Feng, L. Lu, Z. Zhu, R. Wang, and L. Chen. 2016. Methylation-associated silencing of microRNA-129-3p promotes epithelial-mesenchymal transition, invasion and metastasis of hepatocelluar cancer by targeting Aurora-A. Oncotarget 7:78009–78028.

Dixon, S. J., K. M. Lemberg, M. R. Lamprecht, R. Skouta, E. M. Zaitsev, C. E. Gleason, D. N. Patel, A. J. Bauer, A. M. Cantley, W. S. Yang, B. Morrison 3rd, and B. R. Stockwell. 2012. Ferroptosis: an iron-dependent form of non-apoptotic cell death. Cell 149:1060–1072.

Fan, Z., A. K. Wirth, D. Chen, C. J. Wruck, M. Rauh, M. Buchfelder, and N. Savaskan. 2017. Nrf2-Keap1 pathway promotes cell proliferation and diminishes ferroptosis. Oncogenesis 6:e371.

Fei, W., Y. Zhang, Y. Ye, C. Li, Y. Yao, M. Zhang, F. Li, and C. Zheng. 2020. Bioactive metal-containing nanomaterials for ferroptotic cancer therapy. J. Mater. Chem. B 8:10461–10473.

Forcina, G. C., and S. J. Dixon. 2019. GPX4 at the crossroads of lipid homeostasis and ferroptosis. Proteomics 19:e1800311.

Guan, X., Z. Li, S. Zhu, M. Cheng, Y. Ju, L. Ren, G. Yang, and D. Min. 2021. Galangin attenuated cerebral ischemia-reperfusion injury by inhibition of ferroptosis through activating the SLC7A11/GPX4 axis in gerbils. Life Sci. 264:118660.

Han, J., H. Liang, J. Yi, W. Tan, S. He, S. Wang, F. Li, X. Wu, J. Ma, X. Shi, X. Guo, and C. Bai. 2017. Long-term selenium-deficient diet induces liver damage by altering hepatocyte ultrastructure and MMP1/3 and TIMP1/3 expression in growing rats. Biol. Trace Elem. Res. 175:396–404.

Hassannia, B., P. Vandenabeele, and T. Vanden Berghe. 2019. Targeting ferroptosis to iron out cancer. Cancer Cell 35:830–849.

He, Y., Z. Li, T. Xu, D. Luo, Q. Chi, Y. Zhang, and S. Li. 2022. Polystyrene nanoplastics deteriorate LPS-modulated duodenal permeability and inflammation in mice via ROS drived-NF-κB/NLRP3 pathway. Chemosphere 307:135662.

Hu, X., S. Tan, H. Yin, P. A. Khoso, Z. Xu, and S. Li. 2020. Selenium-mediated gga-miR-29a-3p regulates LMH cell proliferation, invasion, and migration by targeting COL4A2. Metallomics 12:449–459.

Imai, H., M. Matsuoka, T. Kumagai, T. Sakamoto, and T. Koumura. 2017. Lipid peroxidation-dependent cell death regulated by GPx4 and ferroptosis. Curr. Top. Microbiol. Immunol. 403:143–170.

Joly, J., A. Delfarah, P. Phung, S. Parrish, and N. Graham. 2020. A synthetic lethal drug combination mimics glucose deprivation-induced cancer cell death in the presence of glucose. J. Biol. Chem. 295:1350–1365.

Kim, D. H., W. D. Kim, S. K. Kim, D. H. Moon, and S. J. Lee. 2020. TGF-β1-mediated repression of SLC7A11 drives vulnerability to GPX4 inhibition in hepatocellular carcinoma cells. Cell Death Dis. 11:406.

Kong, L., and Z. Song. 2021. Organic selenium vs. its combination with sodium selenite in poultry nutrition: food for thoughts - Reply. Poult. Sci. 100:101317.

Koppula, P., Y. Zhang, L. Zhuang, and B. Gan. 2018. Amino acid transporter SLC7A11/xCT at the crossroads of regulating redox homeostasis and nutrient dependency of cancer. Cancer Commun. (Lond) 38:12.

Koppula, P., L. Zhuang, and B. Gan. 2021. Cystine transporter SLC7A11/xCT in cancer: ferroptosis, nutrient dependency, and cancer therapy. Protein Cell 12:599–620.

Kuria, A., H. Tian, M. Li, Y. Wang, J. Aaseth, J. Zang, and Y. Cao. 2020. Selenium status in the body and cardiovascular disease: a systematic review and meta-analysis. Crit. Rev. Food Sci. Nutr. 15:1–10.

Kwon, M., E. Park, S. Lee, and S. Chung. 2015. Heme oxygenase-1 accelerates erastin-induced ferroptotic cell death. Oncotarget 6:24393–24403.

Lan, B., J. W. Ge, S. W. Cheng, X. L. Zheng, J. Liao, C. He, Z. Q. Rao, and G. Z. Wang. 2020. Extract of Naotaifang, a compound Chinese herbal medicine, protects neuron ferroptosis induced by acute cerebral ischemia in rats. J. Integr. Med. 18:344–350.

Lee, H., F. Zandkarimi, Y. Zhang, J. K. Meena, J. Kim, L. Zhuang, S. Tyagi, L. Ma, T. F. Westbrook, G. R. Steinberg, D. Nakada, B. R. Stockwell, and B. Gan. 2020. Energy-stress-mediated AMPK activation inhibits ferroptosis. Nat. Cell Biol. 22:225–234.

Li, G. X., H. J. Lee, Z. Wang, H. Hu, J. D. Liao, J. C. Watts, G. F. Combs, and J. Lü. 2008. Superior in vivo inhibitory efficacy of methylseleninic acid against human prostate cancer over selenomethionine or selenite. Carcinogenesis 29:1005–1012.

Li, B., and L. Zhang. 2021. CircSETDB1 knockdown inhibits the malignant progression of serous ovarian cancer through

miR-129-3p-dependent regulation of MAP3K3. J. Ovarian Res. 14:160.

Liu, T., L. Jiang, O. Tavana, and W. Gu. 2019. The deubiquitylase OTUB1 mediates ferroptosis via stabilization of SLC7A11. Cancer Res. 79:1913–1924.

Liu, J., S. Wang, Q. Zhang, X. Li, and S. Xu. 2020. Selenomethionine alleviates LPS-induced chicken myocardial inflammation by regulating the miR-128-3p-p38 MAPK axis and oxidative stress. Metallomics 12:54–64.

Liu, T., T. Yang, Z. Xu, S. Tan, T. Pan, N. Wan, and S. Li. 2018. MicroRNA-193b-3p regulates hepatocyte apoptosis in selenium-deficient broilers by targeting MAML1. J. Inorg. Biochem. 186:235–245.

Miao, Z., Z. Miao, X. Teng, and S. Xu. 2022. Chlorpyrifos triggers epithelioma papulosum cyprini cell pyroptosis via miR-124-3p/CAPN1 axis. J. Hazard. Mater. 424:127318.

Mou, Y., J. Wang, J. Wu, D. He, C. Zhang, C. Duan, and B. Li. 2019. Ferroptosis, a new form of cell death: opportunities and challenges in cancer. J. Hematol. Oncol. 12:34.

Park, T. J., J. H. Park, G. S. Lee, J. Y. Lee, J. H. Shin, M. W. Kim, Y. S. Kim, J. Y. Kim, K. J. Oh, B. S. Han, W. K. Kim, Y. Ahn, J. H. Moon, J. Song, K. H. Bae, D. H. Kim, E. W. Lee, and S. C. Lee. 2019. Quantitative proteomic analyses reveal that GPX4 downregulation during myocardial infarction contributes to ferroptosis in cardiomyocytes. Cell Death Dis. 10:835.

Payne, R. L., and L. L. Southern. 2005. Changes in glutathione peroxidase and tissue selenium concentrations of broilers after consuming a diet adequate in selenium. Poult. Sci. 84:1268–1276.

Qu, Y., S. Ding, Z. Ma, D. Jiang, X. Xu, Y. Zhang, A. Zhang, and G. Xu. 2019. MiR-129-3p favors intracellular BCG survival in RAW264.7 cells by inhibiting autophagy via Atg4b. Cell. Immunol. 337:22–32.

Rederstorff, M., A. Krol, and A. Lescure. 2006. Understanding the importance of selenium and selenoproteins in muscle function. Cell. Mol. Life Sci. 63:52–59.

Tang, X., X. Fan, T. Xu, Y. He, Q. Chi, Z. Li, and S. Li. 2022. Polystyrene nanoplastics exacerbated lipopolysaccharide-induced necroptosis and inflammation via the ROS/MAPK pathway in mice spleen. Environ. Toxicol. 37:2552–2565.

Wang, F., C. Xu, E. A. Reece, X. Li, Y. Wu, C. Harman, J. Yu, D. Dong, C. Wang, P. Yang, J. Zhong, and P. Yang. 2017. Protein kinase C-alpha suppresses autophagy and induces neural tube defects via miR-129-2 in diabetic pregnancy. Nat. Commun. 8:15182.

Wu, C. T., J. S. Deng, W. C. Huang, P. C. Shieh, M. I. Chung, and G. J. Huang. 2019. Salvianolic acid C against acetaminophen-induced acute liver injury by attenuating inflammation, oxidative stress, and apoptosis through inhibition of the Keap1/Nrf2/HO-1 signaling. Oxid. Med. Cell Longev. 2019:9056845.

Xia, W. G., Z. H. Huang, W. Chen, A. M. Fouad, K. F. M. Abouelezz, K. C. Li, X. B. Huang, S. Wang, D. Ruan, Y. N. Zhang, and C. T. Zheng. 2022. Effects of maternal and progeny dietary selenium supplementation on growth performance and antioxidant capacity in ducklings. Poult. Sci. 101:101574.

Xu, S., L. Xiaojing, S. Xinyue, C. Wei, L. Honggui, and X. Shiwen. 2021. Pig lung fibrosis is active in the subacute CdCl (2) exposure model and exerts cumulative toxicity through the M1/M2 imbalance. Ecotoxicol. Environ. Saf. 225:112757.

Ye, J., Y. Lin, Y. Yu, and D. Sun. 2020. LncRNA NEAT1/microRNA-129-5p/SOCS2 axis regulates liver fibrosis in alcoholic steatohepatitis. J. Transl. Med. 18:445.

Zhang, Z. B., Y. F. Guo, C. Y. Li, C. W. Qiu, and M. Y. Guo. 2019. Selenium influences mmu-miR-155 to inhibit inflammation in Staphylococcus aureus-induced mastitis in mice. Food Funct. 10:6543–6555.

Zhang, H., Y. He, J. Wang, M. Chen, J. Xu, M. Jiang, Y. Feng, and Y. Gu. 2020. miR-30-5p-mediated ferroptosis of trophoblasts is implicated in the pathogenesis of preeclampsia. Redox Biol. 29:101402.

Zhao, L., Y. Feng, Z. J. Xu, N. Y. Zhang, W. P. Zhang, G. Zuo, M. M. Khalil, and L. H. Sun. 2021b. Selenium mitigated aflatoxin B1-induced cardiotoxicity with potential regulation of 4 selenoproteins and ferroptosis signaling in chicks. Food Chem. Toxicol. 154:112320.

Zhao, H., Y. Wang, Y. Liu, K. Yin, D. Wang, B. Li, H. Yu, and M. Xing. 2021a. ROS-induced hepatotoxicity under cypermethrin: involvement of the crosstalk between Nrf2/Keap1 and NF-κB/iκB-α pathways regulated by proteasome. Environ. Sci. Technol. 55:6171–6183.

Zheng, L., L. Feng, W. Jiang, P. Wu, L. Tang, S. Kuang, Y. Zeng, X. Zhou, and Y. Liu. 2018. Selenium deficiency impaired immune function of the immune organs in young grass carp (Ctenopharyngodon idella). Fish Shellfish Immunol. 77:53–70.

Zou, Y., and M. Kong. 2019. Tetrahydroxy stilbene glucoside alleviates palmitic acid-induced inflammation and apoptosis in cardiomyocytes by regulating miR-129-3p/Smad3 signaling. Cell Mol. Biol. Lett. 24:5.